Large Screen Enabled Tri-port MIMO Handset Antenna for Low LTE Bands

Hanieh Aliakbari, *Graduate Student Member, IEEE*, Liying Nie, and Buon Kiong Lau, *Senior Member, IEEE*

***Abstract*—In recent years, the screen-to-body ratio of mobile handsets has been increasing. Today, the screen nearly fills up the entire front side. Conventionally, the screen is mainly seen as a metallic object that adversely affects antenna performance. In this paper, the large screen is used for the first time to facilitate an additional uncorrelated MIMO port in a tri-port design, for several LTE bands below 1 GHz. To this end, the design procedure explicitly considers the screen together with the terminal chassis, which can be simply modelled as two metal plates. In particular, characteristic mode analysis of the double-plate model enables a sufficient number of resonant modes to be created, tuned and selectively excited to yield three uncorrelated MIMO ports in the low band. Simulation and measurement results are found to be in good agreement. The measured bandwidths of the three ports are 23%, 17% and 21%, respectively. Within the operating band, the measured isolation is above 13 dB, envelope correlation coefficient below 0.16 and average total efficiency above 72%.**

***Index Terms*—Characteristic mode analysis, handset antenna, MIMO systems, mobile antenna, mutual coupling.**

I. Introduction

ONE key technology for increasing the channel capacity (ideal data rate) of wireless communication systems is multiple-input multiple-output (MIMO) system. The capacity of a MIMO system is closely related to the number of the antenna elements, as well as the antenna efficiencies and the correlation of signals among these antennas.

Many MIMO terminal antennas have been proposed for sub-6 GHz cellular bands in recent years. Most of these multiport antenna systems focus on relatively high frequencies (i.e., above 1.71 GHz) [1]-[4]. As one example, the eight-port MIMO antenna in [1] covers the band 1.88–2.62 GHz with pairwise isolation of above 10 dB. This is not only because MIMO was first deployed on a massive scale in the Long Term Evolution (LTE) band around 2.6 GHz. More importantly, it is technically very challenging to design MIMO antenna with high efficiency and low correlation for cellular bands below 1 GHz, e.g., LTE Band 5 (0.824-0.894 GHz) and Band 13 (0.746-0.787). The reason is that such low-band antennas rely on the entire chassis for radiation and wideband behavior, and generally the electrically compact chassis with only one resonant mode (dipole mode along chassis length) cannot support low coupling and correlation desired for multi-port MIMO operation [5]. For example, the quad-element design in [6], which is only intended for dual-port MIMO operation by antenna selection, covers the band 0.75-0.96 GHz. However, the isolation in this band is only above 6 dB and the envelope correlation coefficient (ECC) is as high as 0.75.

Nonetheless, dual-port MIMO antennas with moderate to low coupling/correlation have been successfully designed for frequency bands below 1 GHz [5], [7]-[14], either by having a second self- resonant antenna that does not radiate through the chassis (hence narrowband) [5], [7] or facilitating a second resonant mode in these bands through making use of minor changes in the chassis [8]-[14]. The minor changes include the use of loading strips [8], [9] and a bezel frame [10]-[13], some in combination with a larger chassis width (~80 mm) [12]-[14].

However, no tri-port MIMO antenna has yet been found in the literature for these frequencies. The underlying problem is not only in obtaining low correlation. For example, the dual-port design in [7] can be extended to a well-isolated tri-port design by placing one magnetic antenna at both the top and bottom ends of the chassis, apart from having the conventional electric antenna at one end. This is because two magnetic antennas do not rely on the chassis for radiation and they are sufficiently separated for moderate coupling. However, the magnetic antennas are narrowband (~20 MHz [7]) as they operate "in isolation" of the chassis, and a tuning varactor is needed to cover the operating band. Therefore, the challenge is to find a tri-port solution with sufficient isolation and bandwidth over all three ports for practical applications, without frequency tuning and decoupling structures [14].

Increasing screen-to-body ratio of mobile handsets is one of the trends in modern mobile communication systems – with this ratio going from 30.1% to 93.8% over the last 12 years [15], [16]. As a result, the screen covers nearly the entire front side, except for a few millimeters at the sides [17]. The screen is metal-covered to enhance the structural strength of the screen assembly [17]. In [3], the screen is modeled with only a dielectric plate (i.e., glass with a relative permittivity of 5.5),

Manuscript received March 31, 2020. This work was supported in part by Vetenskapsrådet und Grants No. 2010-00468 and No. 2018-04717.

Hanieh Aliakbari and Buon Kiong Lau are with the Department of Electrical and Information Technology, Lund University, 221 00 Lund, Sweden (e-mails: hanieh.aliakbari_abar@eit.lth.se ; *buon_Kiong.Lau@eit.lth.se).

Li Ying Nie is with the EHF Key Lab of Fundamental Science, School of Electronic Engineering, University of Electronic Science and Technology of China, Chengdu 611731, China. (E-mail: liyingnie@sina.com).

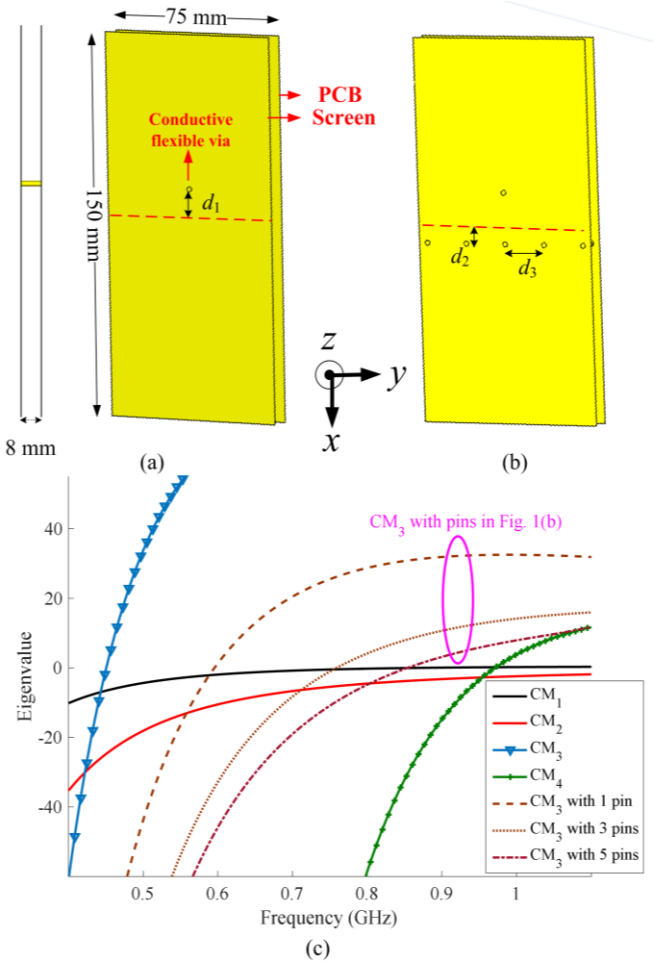

Fig. 1. (a) Geometry and parameters of the connected metal plates (d_1 = 15 mm, d_2 = 5 mm, d_3 = 17 mm), (b) geometry with 5-metal pins added, and (c) Eigenvalues of the modes of interest for the dual-plate model with/without pins.

and hence it has a limited influence on the antenna performance in the 3.5 GHz 5G band. On the other hand, to have a more accurate model, a copper layer has been used in [18] to model the screen. However, the screen-to-body ratio is small (i.e., 45%) and the effect of the screen can, to some extent, be neglected. To the best of the authors' knowledge, there are very few literatures on smartphone antenna design that explicitly accounts for the large metal-covered screen in the design procedure [17], [19].

The effect of the large metal-covered screen was studied in [17] with respect to a metal-framed monopole antenna or planar inverted-F antenna (PIFA) mounted on the top end. It was found that the screen, which in reality is grounded to the terminal chassis, can severely degrade the antenna bandwidth. In [19], the study of the metal-covered screen is extended to design a multi-band single-port antenna, covering GSM850/900, LTE1500, DCS, PCS, UMTS2100, LTE2300/2500, 3.5 GHz 5G bands. Specifically, characteristic mode analysis (CMA) [20] was used to address the bandwidth degradation effect of the large screen observed in [17]. This is because the screen can be included in the design procedure through CMA, and the bandwidth impact can be mitigated by selectively exciting and merging as many resonant characteristic modes (CMs) as possible. However, no effort has so far been made to take advantage of the metal-covered screen to improve smartphone antenna performance, relative to the no-screen chassis model used for antenna design.

In this paper, the large screen is explicitly utilized by CMA to enable the design of a tri-port MIMO antenna below 1 GHz. The design procedure is based on two new resonant modes generated by the addition of the large screen, which facilitates the increase of the number of uncorrelated ports in a previous design [8] from two to three. One of the two new modes was tuned towards the other mode to enable wideband dual-resonance excitation. These two modes were then simultaneously and selectively excited by a single feed (first port) to improve bandwidth and correlation performances, respectively. To prevent the port exciting the loading-strip induced modes from unintentionally exciting the new modes introduced by the screen, a differential feed is utilized for the second port. Finally, the dipole mode along the chassis length is selectively excited by the third port by adding a shorting pin to connect between the top end of the screen and the PCB. The proposed design concept yields at least 17% bandwidth for the tri-port antenna, showing that a tri-port design is feasible from both bandwidth and correlation perspectives even for MIMO operation below 1 GHz. Furthermore, due to theoretical linear capacity increase by the number of uncorrelated antennas, the tri-port design (with ECC below 0.16) is able to support 50% higher data rates for a 3 × 3 MIMO system, as compared to a dual-port design used in a 2 × 2 MIMO system.

II. Large-Screen Induced Modes and Single-Port Excitation

A. CMA of Connected Double-Plate Model

For a large-screen smartphone, the entire metal chassis is more accurately modelled as two connected parallel metal plates, i.e., the screen and the printed circuit board (PCB) (see Fig. 1(a)), instead of just a single PCB (modelled by a single metal plate) as in [1]-[14]. As shown in the smartphone model in Fig. 1(a), there is normally a conductive flexible via (represented by a conductive pin of 1 mm in diameter, located d_1 above the center of each plate) that connects the screen assembly to the PCB [17]. The total model size is 150 × 75 × 8 mm^3, which can be considered typical for popular smartphone models (e.g., Samsung S9 [16]). The addition of a large parallel plate to the single-PCB model is expected to significantly change the CMs of the terminal chassis structure.

In this section, CMA is performed using Altair FEKO [21] to explore the available modes in this connected double-plate chassis, assumed to be a perfect electric conductor (PEC). For the initial analysis, the screen size is set to be the same as the PCB size (see Fig. 1(a)). As also found in [19] for slightly different plate sizes, the new structure of the smartphone chassis will bring different and new resonating CMs in comparison with a single PEC plate of the same dimension (see Fig. 1(c)). The first mode (CM_1) in Fig. 1(c) is the longitudinal half wavelength (0.5λ) dipole mode and the second one (CM_2) is the transversal 0.5λ-dipole mode, both of which also exist in single-PCB models. The lowest-order mode (CM_3) is a

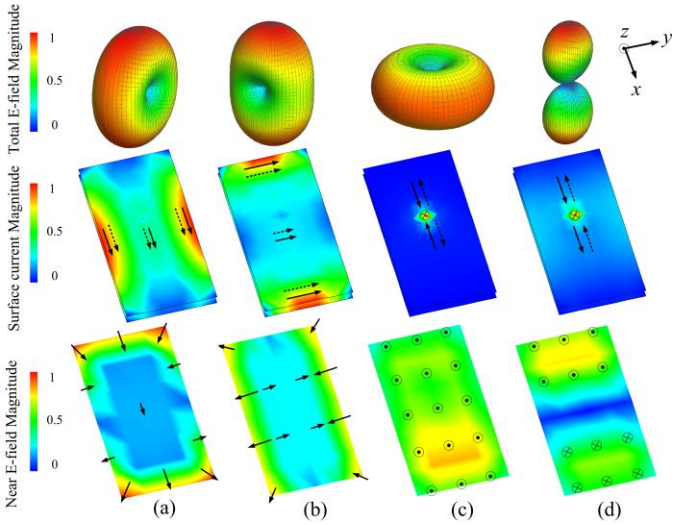

Fig. 2. The normalized farfield patterns, surface currents on the two plates and electric near-field in between two plates for (a) CM_1, (b) CM_2, (c) CM_3, and (d) CM_4 at their respective resonance frequencies. "⊙" and "⊗" represent E-field in positive and negative z directions, respectively. Solid and dashed arrows show the currents on the screen and PCB, respectively.

monopole-like mode that is due to two connected plates and the forth mode (CM_4) is a patch-like mode due to adding the screen at the distance of h to the PCB (h = 8 mm in Fig. 1(a)). The parameter h has little effect on the resonant frequency of the modes in Fig. 1(c).

The characteristic far-field patterns, surface current distributions and electric field (E-field) distribution half-way between the two plates (i.e., the square region 4 mm from either plate) are shown for CM_1-CM_4 in Fig. 2. For CM_3, the surface currents on the screen (upper plate) flows into the metallic pin and then exits the pin into the PCB (lower plate). The directions of the currents are reversed on the two plates and the currents reach a maximum value on the conductive flexible via (pin). The characteristic E-field of CM_3 is almost consistently in the z-direction in the volume between the plates. In contrast, the E-field for CM_4 is in both positive (top half) and negative (bottom half) z-directions, with a minimum E-field magnitude at the middle line. Depending on the position of the conductive flexible via (i.e., d_1 in Fig. 1(a)), the position of the minimum near E-field line of CM_4 can depart from the center. Moreover, the currents for CM_4 is in the same direction over the entire screen, whereas they flow in the opposite direction over the entire PCB. But like CM_3, the currents are maximum along the via. Contrary to CM_3 and CM_4, the directions of the surface currents are the same on the two plates for the CM_1 and CM_2, and the current is minimum on the conductive flexible via. Moreover, the E-field direction between the two plates are along the xy-plane for CM_1 and CM_2.

As shown in Fig. 1(c), the resonance of CM_3 in the initial structure (i.e., 452 MHz) is lower than the desired operating frequency range (~0.8-1.0 GHz). According to the concept in [22], when a circular patch (i.e., two parallel circular plates) is not shorted with a metallic pin, the resonant frequency for the lowest order mode (i.e., TM_{01} or monopole mode in a circular patch antenna) is zero. To increase the resonant frequency of this mode, shorting pins were introduced to shorten the current paths [22]. Similarly, shorting pins can be added between the two plates in the initial structure (see Fig. 1(a)) to increase the resonant frequency of CM_3, resulting in the structure depicted in Fig. 1(b). As shown in Fig. 1(c), as the number of pins increases, the resonant frequency of CM_3 increases. However, the resonances of CM_1 and CM_2 remain unchanged, mainly due to their E-fields not being in the z-direction. To minimize any influence from the pins on the resonance of CM_4, the pins should be positioned along the line of minimum E-field magnitude for CM_4. As mentioned earlier, the minimum E-field region of CM_4 depends on d_1 and it can be moved downward from the middle if d_1 increases. Thus, d_1 and d_2 were optimized to tune the resonant frequencies of both CM_3 and CM_4 to the desired band. The result is that d_1 = 15 mm and d_2 = 5 mm for the 5-pin case.

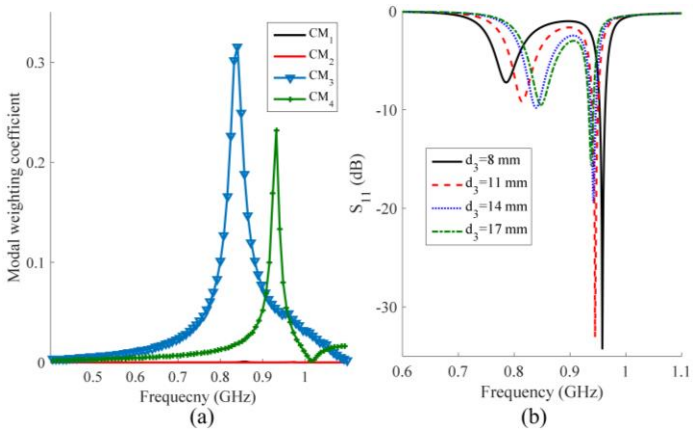

Fig. 3. (a) Modal weighting coefficient of the modes of interest for port 1 excitation, (b) reflection coefficient (S_{11}) for different distance between pins (d_3).

B. Excitation of new CMs by the First Port

Having tuned the resonances of CM_3 and CM_4 to the desired band, the next step is to design the feed to simultaneously excite these two modes to achieve a wideband dual-resonance, based on the 5-pin model. By comparing the characteristic currents and E-fields of modes with small eigenvalues within the desired frequency range (0.8-1.0 GHz) in Fig. 1(c), it can be seen that the currents of CM_3 and CM_4 have similar behavior along the conductive flexible via (i.e., maximum and in the same negative z-direction). So a single feed at that location should be able to simultaneously excite CM_3 and CM_4, leading to a wideband dual-resonance. Moreover, using this single feed should not excite either CM_1 or CM_2, as their currents are very small along the via (see Figs. 2(a) and 2(b)). The selective excitation of CM_3 and CM_4 was verified by calculating the modal weighting coefficients for this port (port 1), which are shown in Fig. 3(a). This strategy also allows CM_1 and CM_2 to be used for other ports, and low correlation with other ports is guaranteed as long as they do not excite CM_3 and CM_4.

As shown in Fig. 3(b), as the distance between the pins (i.e., d_3) increases, the resonant frequency of CM_3 decreases and that of CM_4 remains almost unchanged. The latter is due to the pins being located in a region of low E-field for CM_4. Finally, both modes were matched using BetaMatch [24]. To match the ports,

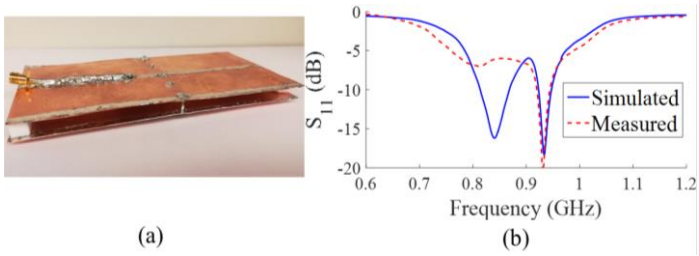

Fig. 4. (a) Prototype of the single-port antenna, (b) measured and simulated S_{11}.

three-element ∏ matching network consisting of a series Murata capacitor and two parallel Murata inductors were used (see Fig. 8(b)). To validate this new concept, a prototype of the optimized single-port antenna was fabricated (see Fig. 4(a)). As shown in Fig. 4(b), 20% bandwidth (792-968 MHz) is achieved with this matching network.

III. Analysis and Excitation of Other Resonant Modes

In principle, the remaining tasks in designing the proposed tri-port MIMO antenna are to ensure that CM_1 and CM_2, similar in modal properties to the resonant modes utilized by the single-PCB dual-port design in [8], are selectively excited by two individual ports (ports 2 and 3). However, unlike in [8], the port design for CM_1 and CM_2 must also avoid exciting CM_3 and CM_4, which are used by port 1.

A. Tuning and Selective Excitation of CM_2 by the Second Port

For the connected double-plate chassis, CM_2 has a transversal 0.5λ-dipole far-field pattern (see Fig. 2(b)) and a resonant frequency well above 1 GHz (see Fig. 1(c)). To reduce the resonant frequency to below 1 GHz, the structure can be capacitive loaded along the longer sides of the PCB plate with two center-grounded metal strips (see Fig. 5(a)), as performed in [8] for the conventional single-PCB model. The dimensions of each strip is 150 mm × 5 mm, and they are placed 3 mm above the sides of the PCB. This PCB modification lowers the resonant frequency of CM_2 with respect to Fig. 1(c). Moreover, it can be seen in Fig. 5(b) that as the clearance between the screen and the strips is increased, the slope of the eigenvalue of CM_2 decreases. Thus, to ensure that the potential bandwidth of port 2 is acceptable, the screen width W_s is reduced from 75 mm to 70 mm. It is noted that, by these structure modifications, the far-field pattern of each mode remains the same as that of the original double-plate structure (see Fig. 2). However, the characteristic currents are slightly modified due to the two loading strips. For instance, the modified currents of CM_2 and CM_3 are illustrated in Figs. 6(a) and 6(b), respectively.

To excite CM_2, the feeding port can be placed at a high-current location. One such location is any one of the two shorting pins for the loading strips, as can be seen in Fig. 6(a). Through replacing one of the two shorting pins with a gap feed port, the modal weighting coefficient is calculated and plotted in Fig. 7(a). It can be seen that, by adding one feed, CM_2 will be excited. Moreover, the center location of the feed along the strip helps to prevent the excitation of CM_1 and CM_4 due to their low E-fields at this location, as shown in Figs. 2(a) and 2(d). Nonetheless, as shown in Fig. 7(a), CM_3 has also been excited

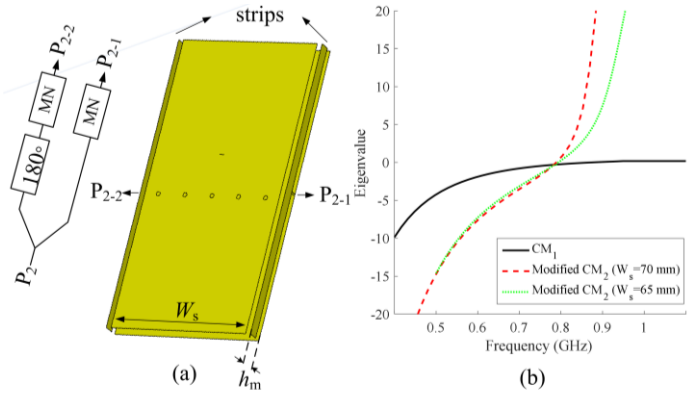

Fig. 5. (a) Connected plates with metal strips and the feeding network consisting of a power divider with a 180° phase difference in the output ports and matching networks (MN) (W_s = 70 mm, h_m = 7 mm), (b) modified eigenvalue for different screen sizes.

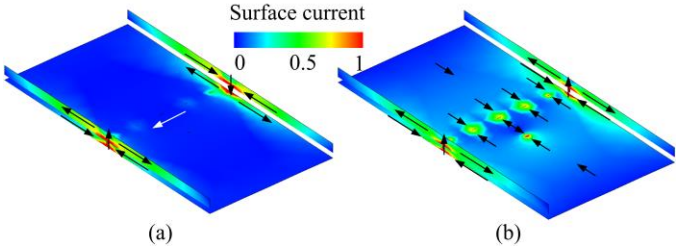

Fig. 6. Modified surface currents by adding two grounded loading strips for (a) CM_2, and (b) CM_3. For clarity, the screen and connecting pins are not shown.

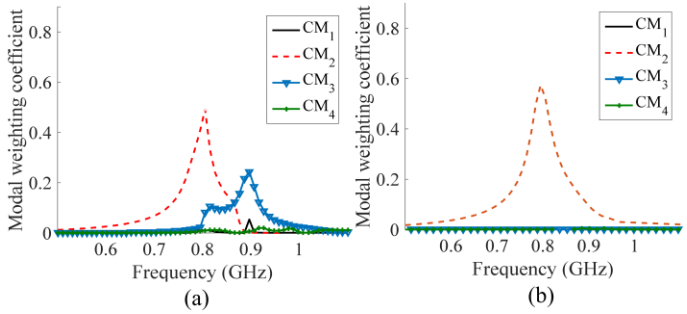

Fig. 7. Modal weighting coefficient of the modes for port 2 and with: (a) one feed, and (b) two feeds with 180° phase shift (W_s = 70 mm). The feed power is kept equal in both cases.

by this feed, as it has a high-current at that locations, as shown in Fig. 6(b).

To selectively excite only CM_2, the currents of CM_2 and CM_3 (in Figs. 6(a) and 6(b), respectively) were compared. It can be seen that, although the currents on the shorting pins (of the metal strips) flow in different directions for CM_2 they are in the same direction for CM_3. Thus, instead of exciting CM_2 with only one feed, the other pin is also replaced with a feed, with a new port (port 2) feeding them with a 180° phase difference to ensure no excitation of CM_3 (see Fig. 5(a)). The resulting modal weighting coefficient in Fig. 7(b) reveals that CM_3 is no longer excited with this differential feeding scheme.

Each of the ports in Fig. 5(a) was matched in BetaMatch [24] using 4-element cascaded Murata components (see Fig. 8(b)), which yields a 6 dB impedance bandwidth of 15% (830-960

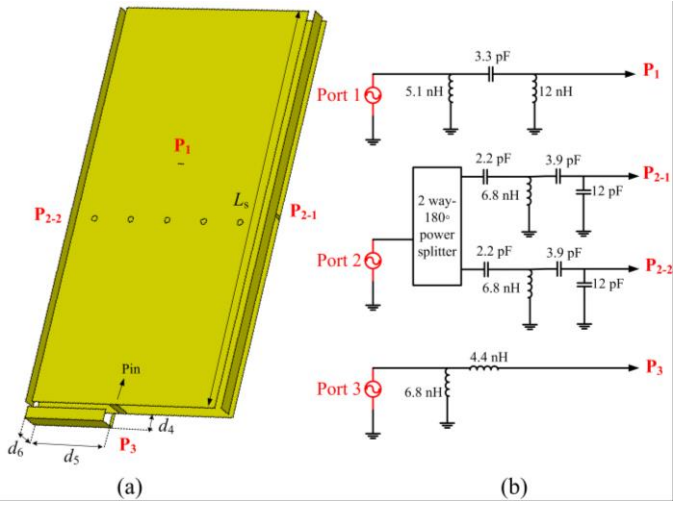

Fig. 8 (a) Antenna structure with one CCE (d_4 = 5 mm, d_5 = 30 mm, d_6 = 6 mm, L_s = 145 mm), (b) matching networks consisting of Murata components connected to the ports.

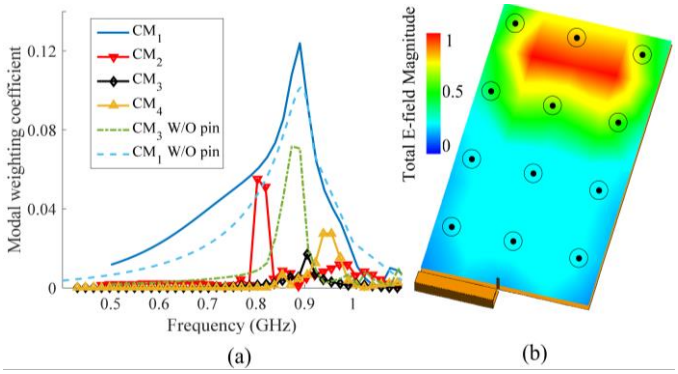

Fig. 9 (a) Modal weighting coefficient of the modes for port 3 and, (b) electric near-field of the CM_3 mode (half-way between the screen and the PCB) after adding a shorting pin close to the single CCE.

MHz) as depicted in Fig. 11. It is noted that, as the width of the screen W_s decreases, the number of elements needed to match the loading strip port (port 2) is smaller. In addition, as the distance of the screen to the PCB h together with the strip height (h_m) increases, the impedance bandwidth of the port improves.

B. Tuning and Selective Excitation of CM_1 by the Third Port

Considering the E-field distribution of CM_1 in Fig. 2(a), it is common to use one capacitive coupling element (CCE) at a corner of the PCB to excite this mode [23]. To keep the overall length of the structure constant at 150 mm upon adding the CCE, the length of the double-plate model is reduced by 5 mm. The modal weighting coefficients of CM_1-CM_4 for a single CCE utilized as the third port are shown in Fig. 9(a). It can be seen in Fig. 9(a) that CM_3 is also excited by the CCE, whereas other modes are only slightly excited in the band of interest. To remedy this problem, a shorting pin was added between the screen and the PCB at the top center position, near the position of the CCE. This solution was motivated by the E-field behavior seen in Fig. 2, i.e., the E-field of CM_3 is z-oriented whereas that of CM_1 is oriented along the xy-plane. Therefore, the added pin shorted out the E-field of CM_3 in this region (see Fig. 9(b)), without affecting that of CM_1, such that the excitation of CM_3

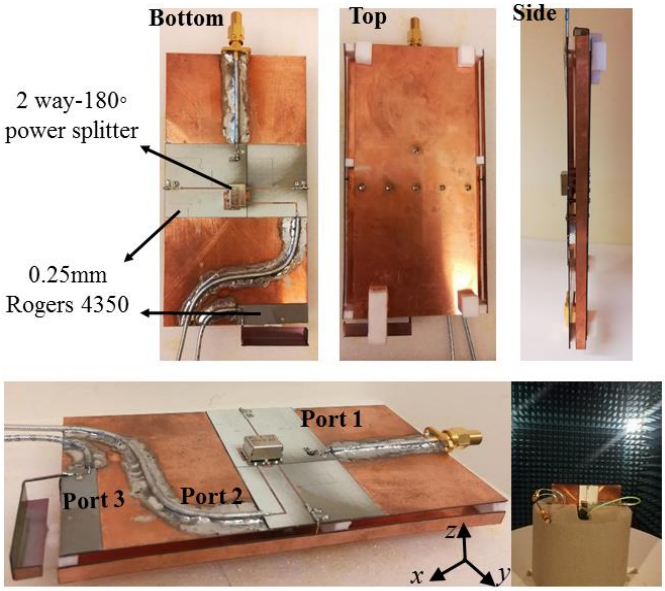

Fig. 10. Prototype of the proposed tri-port MIMO antenna shown with different viewing angles, and it being mounted for pattern measurement (bottom right).

notably decreased, as shown in Fig. 9(a). To match the CCE for port 3, a two-element L matching network with two Murata inductors was used, resulting in the 6 dB bandwidth of 790-960 MHz, as shown in Fig. 11. If the length of the screen L_s is increased beyond 145 mm, the bandwidth of this port will be reduced [17]. Thus for the final configuration shown in Fig. 8(a), the screen to body ratio is around 90%.

It should be noted that only one CCE is used to excite CM_1 in this work (see Fig. 8(a)), to achieve a compact implementation and allow for more space for possible higher band antennas. Previous studies have demonstrated that, as the number of properly phased and positioned CCEs (for exciting CM_1) increases, the required complexity of the matching network to attain a certain bandwidth decreases [23]. Furthermore, multiple CCEs will facilitate more selective excitation of CM_1, potentially reducing coupling with the other two ports.

IV. Experimental Results

To validate the proposed design concept, a prototype of the tri-port double-plate structure was fabricated (see Fig. 10). Two 0.3 mm thick copper plates were used to implement the PCB and the screen. The feeding networks were etched on a 0.25 mm Rogers 4350 substrate with the relative permittivity of 3.48, as shown in Fig. 10. To excite the two strips from middle with the same magnitude and 180◦ phase difference, a surface mount 2 way-180◦ power splitter (Mini-circuits SYPJ-2-222+) was used. To ease the implementation of the feeding networks, the substrate is attached on the bottom side of the PCB by using a conductive glue. In real applications, it can also be placed between the two plates.

Figure 11 shows the simulated and measured S-parameters of the proposed tri-port terminal antenna. As can be seen, the isolation between ports 3 and 1, or ports 3 and 2, is lower than that between ports 1 and 2. As mentioned earlier, this is because

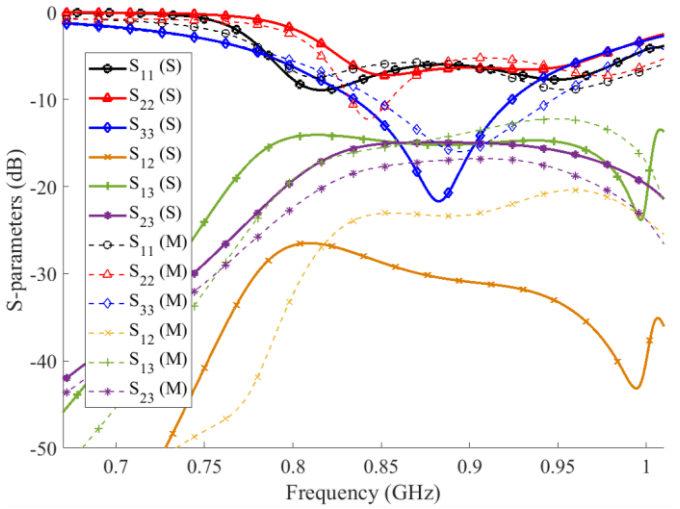

Fig. 11. Simulated (S) and measured (M) S-parameters of the tri-port antenna.

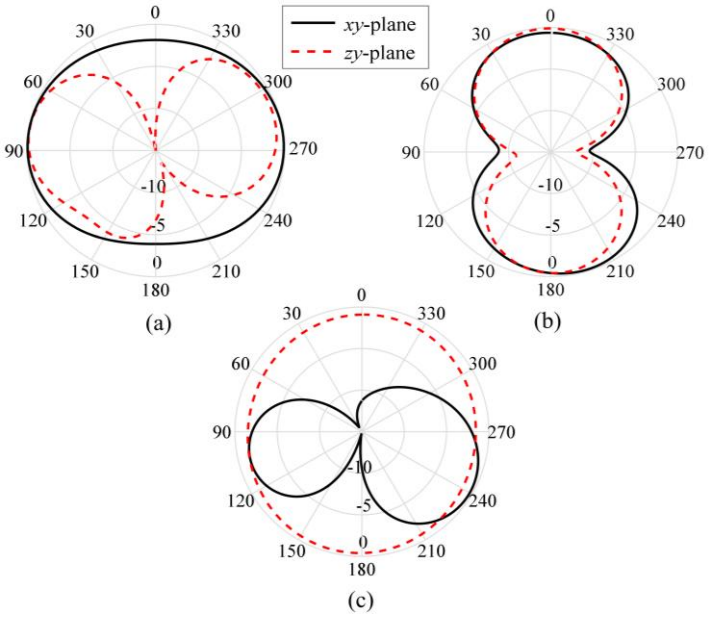

Fig. 12. Measured radiation patterns of (a) port 1, (b) port 2, and (c) port 3 in *xy*- and *yz*-planes at 0.9 GHz, individually normalized at each port.

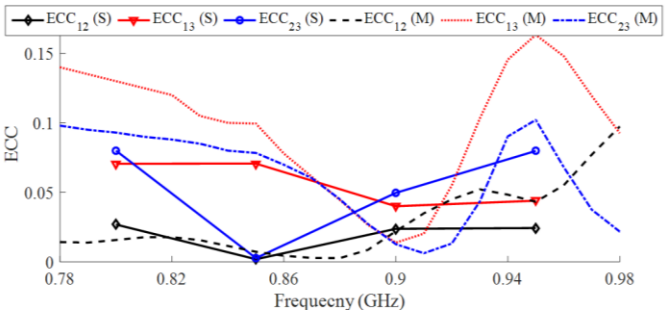

Fig. 13. Simulated (S) and measured (M) far-field ECC of the tri-port antenna.

the CCE of port 3 will partially excite the other modes, as illustrated earlier in Fig. 9(a). Nevertheless, the measured isolation of over 13 dB, 20 dB, 17 dB is achieved in S_{13}, S_{12} and S_{23}, respectively, which are generally considered as low enough for mobile terminal applications involving frequencies lower than 1 GHz (e.g., [5]-[14]). The 6 dB impedance bandwidth of the first, second and third ports are 23% (0.79-1 GHz), 17% (0.82-0.98 GHz), and 21% (0.8-0.98 GHz), respectively. Relatively good agreement between the simulated and measured bandwidths can be observed. The measured S_{11} and S_{22} has slightly larger bandwidths than the simulated ones, but the in-band matching is slightly worse. S_{33} is slightly shifted at higher frequencies, but it still covers the targeted band.

The radiation parameters of the fabricated prototype were obtained from a multi-probe spherical near-field system. The measured far- field patterns of the three ports at 0.9 GHz are given in Fig. 12 in two planes. As expected, it can be observed that the total radiation patterns of the first, second and third ports at 0.9 GHz are very similar to the far-field patterns of CM_3, CM_2, and CM_1, respectively (see Fig. 2), since each port was designed to selectively excite one of these modes. The contribution from CM_4 to the pattern of port 1 only becomes more prominent at higher frequencies, as it contributes to the second (higher) resonance of port 1. The minor differences between the radiation patterns of the fabricated prototype and those of the CMs are primarily due to the presence of a feeding cable, connected to the three SMA connectors on the bottom of the antenna, which was in the near field of the structure during the measurement. Other factors contributing to these minor differences include tolerances in the fabrication and possible small phase/amplitude imbalances of the power splitter used in the prototype. The ECC, as obtained from measured far-field patterns, is below 0.16 for all the three ports, as shown in Fig. 13. The average measured total efficiencies of the first, second, and third ports in their operating bandwidths of the antenna are 74%, 72%, and 80%, respectively. The total efficiencies of the three ports are over 70% in the common bandwidth (i.e., 0.82-0.98 GHz). The efficiency values are affected by the losses of. the power splitters and the feeding networks

To provide more insight into the system performance and the respective contributions from the total efficiencies and ECCs of the three ports, multiplexing efficiency [25] can be used. Essentially, it is an equivalent power loss (for a given MIMO capacity) due to non-perfect total efficiencies and non-zero correlation. Hence, it can be seen as a multi-antenna extension of the single-port total efficiency concept. For a high signal-to-noise ratio (required for MIMO multiplexing transmission) and the reference channel with uniform 3D angular power spectrum, the multiplexing efficiency for a *M*-port MIMO antenna is given by the compact form [25]

$$\eta_{mux} = \left(\prod_{k=1}^{M} \eta_k\right)^{1/M} \det(\mathbf{R})^{1/M} \tag{1}$$

where η_k is the total efficiency of port k, $\mathbf{R}$ is the correlation matrix, det(.) is the determinant operator and $\prod$ is the product operator. $\mathbf{R}$ for a tri-port antenna is

$$\mathbf{R} = \begin{bmatrix} 1 & \rho_{12} & \rho_{13} \\ \rho_{12}^* & 1 & \rho_{23} \\ \rho_{13}^* & \rho_{23}^* & 1 \end{bmatrix}, \tag{2}$$

and ρ_{mn} is the complex correlation coefficient of the far-field patterns for ports m and n [25]. For the proposed tri-port

antenna, the minimum η_{mux} is calculated to be 67.0% (-1.74 dB) in the common bandwidth. Based on (1), the contributions from antenna efficiencies and correlations (left vs. right terms) to η_{mux} are -1.37 dB and -0.37 dB, respectively, indicating that the efficiency performance dominates and the ECC values are low enough to not have any major impact on the achieved MIMO performance.

V. Conclusions

Based on new modes introduced by the large metal-covered screen, a tri-port MIMO antenna is proposed for the first time for large-screen smartphones, to cover cellular bands below 1 GHz. The proposed antenna is implemented without any decoupling structure and with the spacing between the feeding locations limited to half the chassis length. The strategy of identifying and selectively exciting available modes facilitates high total efficiencies (above 70%) and low ECC (below 0.16) within the operating bandwidth. One possible future work is to enhance the bandwidth of some ports.

Acknowledgment

The authors would like to thank Andreas Johansson at Lund University for his help in fabricating the antenna prototypes and Dymtro Pugachev of Sigma Connectivity AB for his help in the pattern measurement.

References

[1] Z. Qin, W. Geyi, M. Zhang, and J. Wang, "Printed eight-element MIMO system for compact and thin 5G mobile handset," *Electron. Lett.*, vol. 52, no. 6, pp. 416–418, Mar. 2016.

[2] D. Changjiang, and X. Lv, "Wideband MIMO antenna with small ground clearance for mobile terminals," *IET Microw. Antennas Propag.*, vol. 13, no. 9, pp. 1419–1426, 2019.

[3] L. Sun, H. Feng, Y. Li, and Z. Zhang, "Compact 5G MIMO mobile phone antennas with tightly arranged orthogonal-mode pairs," *IEEE Trans. Antennas Propag.*, vol. 66, no. 11, pp. 6364–6369, Nov. 2018.

[4] J. Guo, L. Cui, C. Li, and B. Sun, "Side-edge frame printed eight-port dual-band antenna array for 5G smartphone applications," *IEEE Trans. Antennas Propag.*, vol. 66, no. 12, pp. 7412–7417, Dec. 2018.

[5] H. Li, Y. Tan, B. K. Lau, Z. Ying, and S. He, "Characteristic mode based tradeoff analysis of antenna-chassis interactions for multiple antenna terminals," *IEEE Trans. Antennas Propag.*, vol. 60, no. 2, pp.409–502, Feb. 2012.

[6] S. Zhang, K. Zhao, Z. Ying, and S. He, "Adaptive quad-element multi wideband antenna array for user-effective LTE MIMO mobile terminals," *IEEE Trans. Antennas Propag.*, vol. 61, no. 8, pp. 4275–4283, Aug. 2013.

[7] H. Li, B. K. Lau, Z. Ying, and S. He, "Decoupling of multiple antennas in terminals with chassis excitation using polarization diversity, angle diversity and current control," *IEEE Trans. Antennas Propag.*, vol. 60, no. 12, pp. 5947-5957, Dec. 2012.

[8] H. Li, Z. Miers, and B. K. Lau, "Design of orthogonal MIMO handset antennas based on characteristic mode manipulation at frequency bands below 1 GHz," *IEEE Trans. Antennas Propag.*, vol. 62, no. 5, pp. 2756–2766, May 2014.

[9] Z. Miers, H. Li, and B. K. Lau, "Design of bandwidth enhanced and multiband MIMO antennas using characteristic modes," *IEEE Antennas Wireless Propag. Lett.*, vol. 12, pp. 1696–1699, Nov. 2013.

[10] Z. Miers, H. Li, and B. K. Lau, "Design of bezel antennas for multiband MIMO terminals using characteristic modes," in *Proc. 8th Europ. Conf. Antennas Propag. (EuCAP'2014)*, The Hague, The Netherlands, Apr. 6-10, 2014, pp. 2556-2560.

[11] K. K. Kishor, and S. V. Hum, "Multiport multiband chassis-mode antenna design using characteristic modes," *IEEE Antennas Wireless Propag. Lett.*, vol. 16, pp. 609-612, 2017.

[12] I. Barani, and K. Wong, "Integrated inverted-F and open-slot antennas in the metal-framed smartphone for 2 x 2 LTE LB and 4 x4 LTE M/HB MIMO operations," *IEEE Trans. Antennas Propag.*, vol. 66, no. 10, pp. 5004–5012, Oct. 2018.

[13] D. Huang, Z. Du, and Y. Wang, "A quad-antenna system for 4G/5G/GPS metal frame mobile phones." *IEEE Antennas and Wireless Propag. Lett.*, vol. 18, pp. 1586-1590, 2019.

[14] S. Wang and Z. Du, "Decoupled dual-antenna system using crossed neutralization lines for LTE/WWAN smartphone applications," *IEEE Antennas Wireless Propag. Lett.*, vol. 14, pp. 523–526, 2015.

[15] J. Callaham, "The race to 100 percent: Smartphone screen-to body ratios over the years." [Online]. Available: https://www.androidauthority.com/smartphone-screen-to-bodyratio-878835/.

[16] "Specifications | Samsung Galaxy S9 and S9+," The Official Samsung Galaxy Site. [Online]. Available: https://www.samsung.com/global/galaxy/galaxy-s9/specs/.

[17] B. Xiao, H. Wong, B. Wang, and K. L. Yeung, "Effect of the screen to metal-frame smartphone antennas," *IEEE Int. Workshop Antenna Technol. (iWAT)*, Miami, FL, Mar. 3-6, 2019, pp. 29-32.

[18] K. Payandehjoo, and R. Abhari, "Compact multi-band PIFAs on a semi-populated mobile handset with tunable isolation," *IEEE Trans. Antennas Propag.*, vol. 61, no. 9, pp. 4814-4819, Sep. 2013.

[19] B. Xiao, H. Wong, D. Wu, and K. L. Yeung, "Metal-frame antenna for big-screen smartphones using characteristic mode analysis," *IEEE Access*, vol. 7, pp. 122224-122231, 2019.

[20] R. Harrington and J. Mautz, "Theory of characteristic modes for conducting bodies," *IEEE Trans. Antennas Propag.*, vol. AP-19, no. 5, pp. 622–628, Sep. 1971.

[21] Altair FEKO, version 2018 (2018). Altair Engineering, Inc. Accessed: Mar. 16, 2020. [Online]. Available: https://altairhyperworks.com/product/FEKO.

[22] J. Liu, Q. Xue, H. Wong, H. W. Lai, and Y. L. Long, "Design and analysis of a low-profile and broadband microstrip monopolar patch antenna," *IEEE Trans. Antennas Propag.*, vol. 61, no. 1, pp. 11–18, Jan. 2013.

[23] H. Aliakbari and B. K. Lau, "On modal excitation using capacitive coupling elements and matching network," *in Proc. IEEE Int. Symp. Antennas Propag. (APS'2019)*, Atlanta, GA, Jul. 7-12, 2019.

[24] Betamatch, version 3.7.6. (2019). MNW Scan Pte Ltd. Accessed: Mar. 16, 2020. [Online]. Available: http://www.mnw-scan.com/.

[25] R. Tian, B. K. Lau, and Z. Ying, "Multiplexing efficiency of MIMO antennas," *IEEE Antennas Wireless Propag. Lett.*, vol. 10, pp. 183–186, 2011.